Proceedings of Maglev 2024

7976-A-2466

Comparison of Permanent Magnet Configurations of an Electrodynamic Suspension Integrated in a Small-Scale Test Vehicle

Louis Beauloye, Institute of Mechanics, Materials and Civil Engineering, UCLouvain, Louvain-La-Neuve, Belgium, louis.beauloye@uclouvain.be.

David Melly, Institute of Systems Engineering, School of Engineering, HES-SO Valais-Wallis, Sion, Switzerland.

Samuel Chevailler, Institute of Systems Engineering, School of Engineering, HES-SO Valais-Wallis, Sion, Switzerland.

Bruno Dehez, Institute of Mechanics, Materials and Civil Engineering, UCLouvain, Louvain-La-Neuve, Belgium.

ABSTRACT

Electrodynamic suspensions are well-suited for high-speed maglev systems. This paper optimizes and compares two configurations of permanent magnets of such suspension integrated in a small-scale test vehicle. The first one is the Halbach array, classically used for the high magnetic flux density it generates, whereas the second one is the simpler alternance of magnetic poles. Through the optimization of the lift-to-drag ratio and the mass of the suspension, it is shown that both configurations can have similar performances. The Halbach array has a lower overall mass but a higher permanent magnet volume and therefore cost. A portion of the additional weight of the alternate arrangement can be gained by reducing its back-iron thickness and removing materials at the center of the magnetic poles.

• Keywords: High-speed maglev, electrodynamic suspension (EDS), permanent magnets

1. INTRODUCTION

Relying on the interaction between permanent magnets (PMs) attached to the vehicle and a conductive track, electrodynamic suspension (EDS) are fully passive and therefore offer a simple and robust solution for the magnetic levitation of high-speed maglev [1]. The way permanent magnets are arranged influence greatly the performance of the suspension in terms of efficiency but also building cost. The most studied arrangement is the Halbach configuration [2, 3]. However, the rather simple alternate magnetic pole configuration remains interesting to investigate [4]. The latter offers an easier construction but at the expense of an added back-iron to close the magnetic flux lines. The goal of this paper is to compare these two topologies when integrated in a specific application, the project GRIPIT [5]. This project consists of the study of several technologies applied to vacuum transportation. Related to the EDS, a demonstrator of about 190kg is developed and will be tested. Both topologies are therefore optimized under the constraints of the application and then compared based on several criteria.

2. MATERIALS AND METHODS

2.1 Global description

The optimized EDS systems will be tested on a small test vehicle developed during the GRIPIT project. The aim of this project is to create a synergistic interaction between the industrial and scientific forces involved in the technologies required for the deployment of surface and underground, partial vacuum and atmospheric pressure transportation systems. In this context, GRIPIT (Interdisciplinary research group for innovative transportation projects) has set itself the mission of putting in place the tools and methodologies to design innovative transport systems on an interdisciplinary basis. The main objectives of GRIPIT are to develop an anthropotechnological / systemic model for the co-design of future transportation systems but also to develop and validate a multiphysics vehicle dynamic model of a tuned EDS with its mechanical suspension and to design and evaluate infrastructure and electromechanical systems for propulsion/levitation.

FIGURE 1: *Test vehicle on its track*

The vehicle is shown in Figure 1 and its main specifications are the following:

- Dimensions of 3 m x 1.2 m
- Weight of 190kg
- Propulsion by an overheated water booster
- Maximum speed of 120 km/h reached in 1 sec
- 100 m long track made of aluminum I-beams
- 4 EDS passive magnetic levitation modules with each a mechanical suspension and a mechanical brake
- Levitation height between 3 and 8 mm.

The completion of the project is planned for August 2024.

2.2 Topologies and parameters

The alternate PM (AltPM) and Halbach array (HA) topologies are illustrated in Figures 2a and 2b respectively. The parameterization of both arrangements is also shown. The particular L-shaped track used in the project is also represented in Figures 2a and 2b. The value of the parameters are listed in Table 1 and 2, separated into the fixed parameters that will stay constant throughout the analyses and the variable parameters which will be optimized. The back-iron thickness t_{ir} of the AltPM is selected to avoid its magnetic saturation based on the magnetic flux going in the iron and a maximum magnetic flux density of 1.5 T. We can therefore conduct only

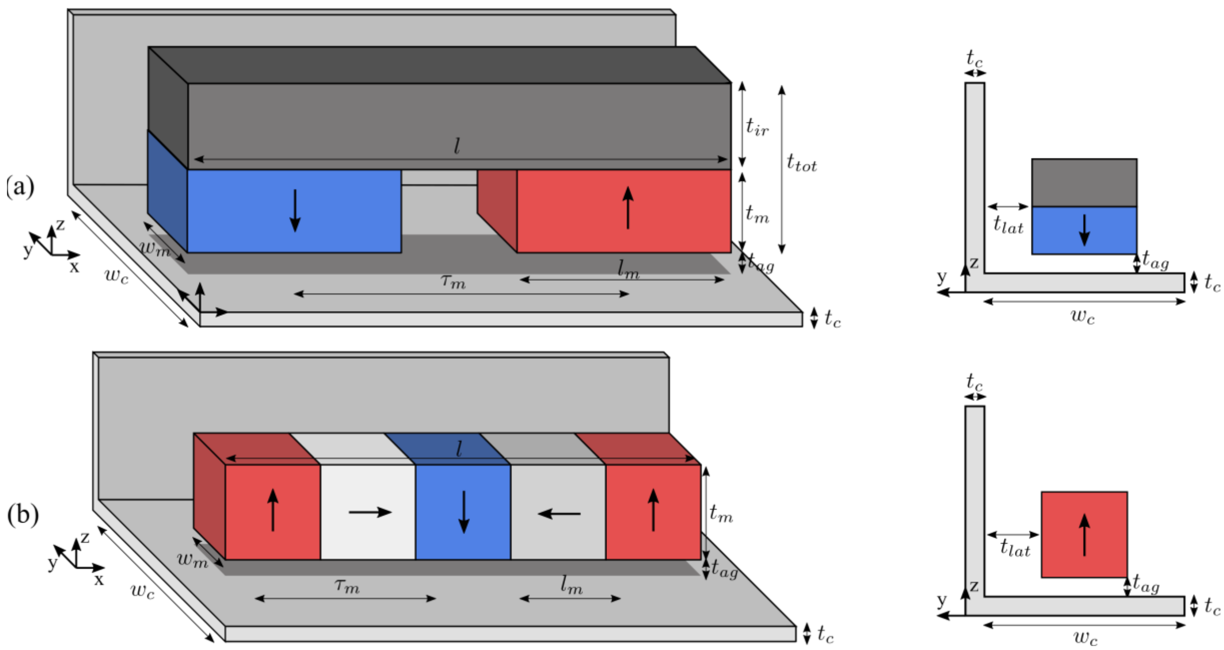

FIGURE 2: *PM-EDS topologies and parameters. (a) Alternate PM. (b) Halbach array*

Parameter	Symbol	Value	Unit
Track width	w_c	70	mm
Track thickness	t_c	10	mm
Track conductivity	σ_c	$3.03 \cdot 10^7$	S/m
Air gap	t_{ag}	10	mm
PM remanence	B_r	1.37	T
PM permeability	$\mu_{r,m}$	1.06	-
Iron permeability	$\mu_{r,ir}$	2000	-
Speed	v_x	30	m/s

TABLE 1: *Fixed parameters for the optimization*

linear simulations. The lateral gap t_{lat} is equal to $(w_c - w_m)/2$ to keep the PMs centered above the bottom track.

Parameter	Symbol	Min	Max	Unit
Total length	l	100	300	mm
PM thickness	t_m	10	70	mm
PM width	w_m	10	40	mm
Pole pitch	τ_m	10	$l/2$	mm
PM span	l_m/τ_m	0	1	-

TABLE 2: *Optimization parameters*

2.3 Model

Both topologies of PM-EDSs are modeled analytically. This enables us to optimize them efficiently under various conditions and compare them fairly. The 3-D model, based on [6], starts from a resolution of Maxwell's equation in the whole domain separated in continuous regions in the xy-plane. In the conductive plate, it gives:

$$\nabla^2 \boldsymbol{A} = \mu_0 \sigma_c (\boldsymbol{v} \cdot \nabla) \boldsymbol{A} \tag{1}$$

with $\boldsymbol{A}$ the magnetic vector potential. Elsewhere, we have:

$$\nabla^2 \boldsymbol{A} = 0 \tag{2}$$

The PM magnetic field source is used as a boundary condition at the plate interface. It is computed using charge modeling [7, 8] from the superposition of the magnetic field of single PMs.

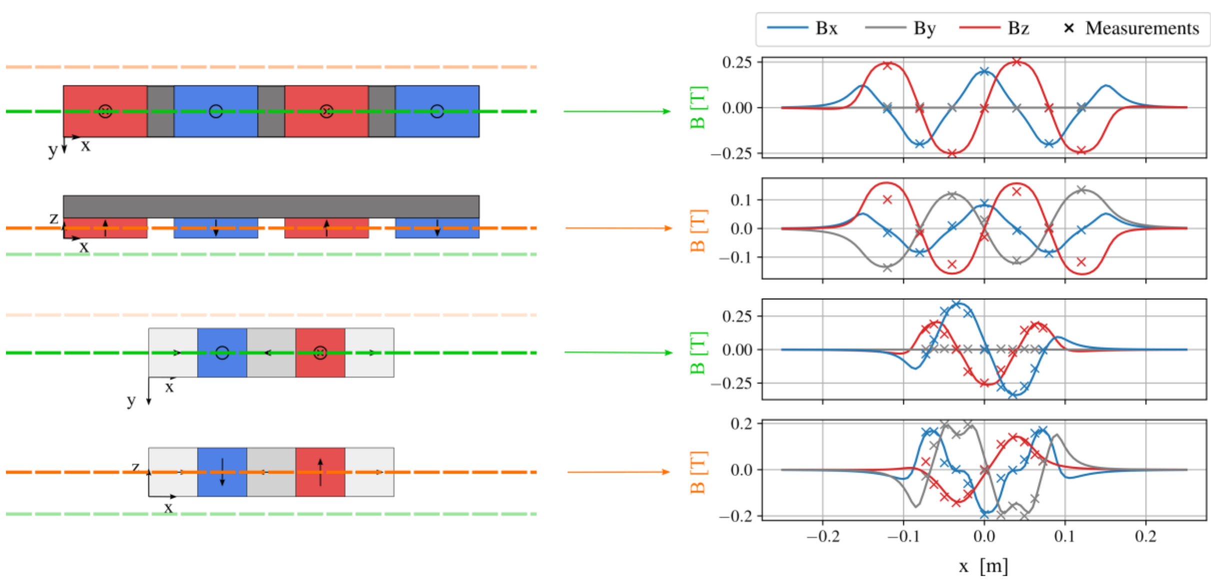

FIGURE 3: *Source magnetic flux density model and measurements for the AltPM and HA. The green line is centered and 15 mm below the array. The orange line is centered on the side of the PMs and 10 mm on the left of the array.*

In Figure 3, the magnetic field source of two arrangements have been measured experimentally and compared to the model along two lines in the x-direction: the green line below the array and the orange line on the side. We can observe a great agreement between the analytical model and the measurements.

Once the magnetic field is known everywhere in the domain after solving (1) and (2), the forces are finally computed using Maxwell's stress tensor.

The forces generated by the track on the side are computed using the same model but with the PMs rotated by 90 degrees along the x-axis.

The model has several limitations. First, the interactions between both tracks is not modeled. Then, the forces linked to the edge effects generated by a decentering of the PMs in the plates are not well considered. Finally, if the width of the track is not large enough compared to the width of the PMs and the pole pitch, the accuracy of the model can be limited. The solutions obtained with this analytical model will be therefore be evaluated using FEM in COMSOL Multiphysics to confirm the results.

2.4 Optimization process

The parameters listed in Table 2 are chosen as optimization variables. Their bounds are selected based on the constraints of the application. Two objectives are maximized in a bi-objective optimization: the lift-to-drag ratio (LDR) and the mass of the suspension. A constraint is imposed on the lift force F_L so as to sustain the whole weight of the vehicle at the rated speed and air gap:

$$F_L \geq \frac{P_v}{4} + P_s \tag{3}$$

where P_v is the weight of the vehicle without the suspension and P_s is the weight of the suspension. P_v is divided by 4 since 4 suspensions are installed in the vehicle. The genetic algorithm NSGA-III is used for the optimization.

3. RESULTS AND DISCUSSION

3.1 Optimization results

The Pareto fronts between mass and LDR for both arrangements obtained after the optimization of one suspension are presented in Figure 4. The topologies behind specific points of the fronts are represented in Figure 5 to better visualize them. It can be first noticed that the optimized Halbach array dominates the alternate PM with a higher LDR and a lower mass. Topologies I and IV, like topologies II and V, are very similar with almost the same pole pitch, PM span and PM thickness. It is logical to a have higher mass for the AltPM since the back-iron add up to the PM weight. However, the LDRs should be equal for the same pole pitch. Table 3 compares the LDRs computed with the analytical model and using FEM. The results show that indeed both topologies I and IV and, II and V have almost equal LDRs. It seems that the limitations of the analytical model introduced in Section 2.3 have a greater impact on the HA than the AltPM arrangements.

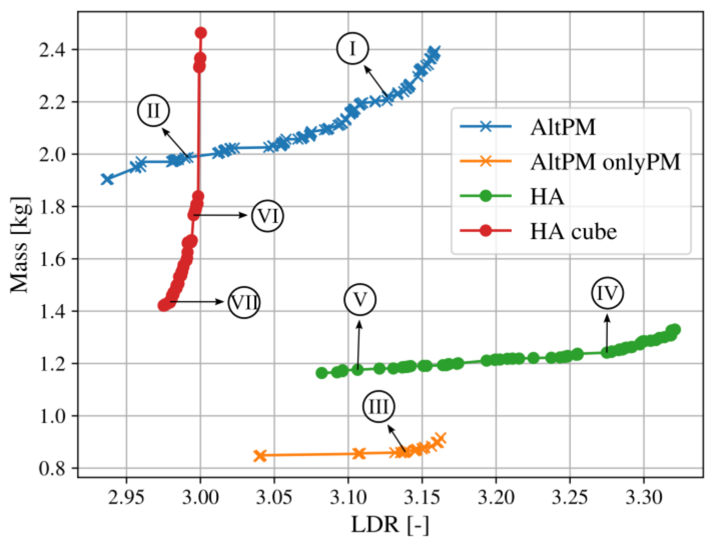

FIGURE 4: *Optimization results*

The AltPM has a lower PM mass than its HA counterpart which can be interesting when the back-iron is part of the vehicle structure. The PMs are also more expensive than the ferromagnetic material. An optimization of the AltPM was therefore conducted while considering only the PMs in the weight of the suspension. By comparing the topologies III and IV in Table 3, it can be seen that, in the orange front, a significantly lower PM mass than the HA can be reached for the same LDR.

The Halbach array is often made with PM cubes to reduce costs and ease the manufacturing. The HA was then optimized while constraining the PM thickness and the PM width to be equal to half the pole pitch, leading to the red front in Figure 4 with a lower LDR and higher mass than the unconstraint HA.

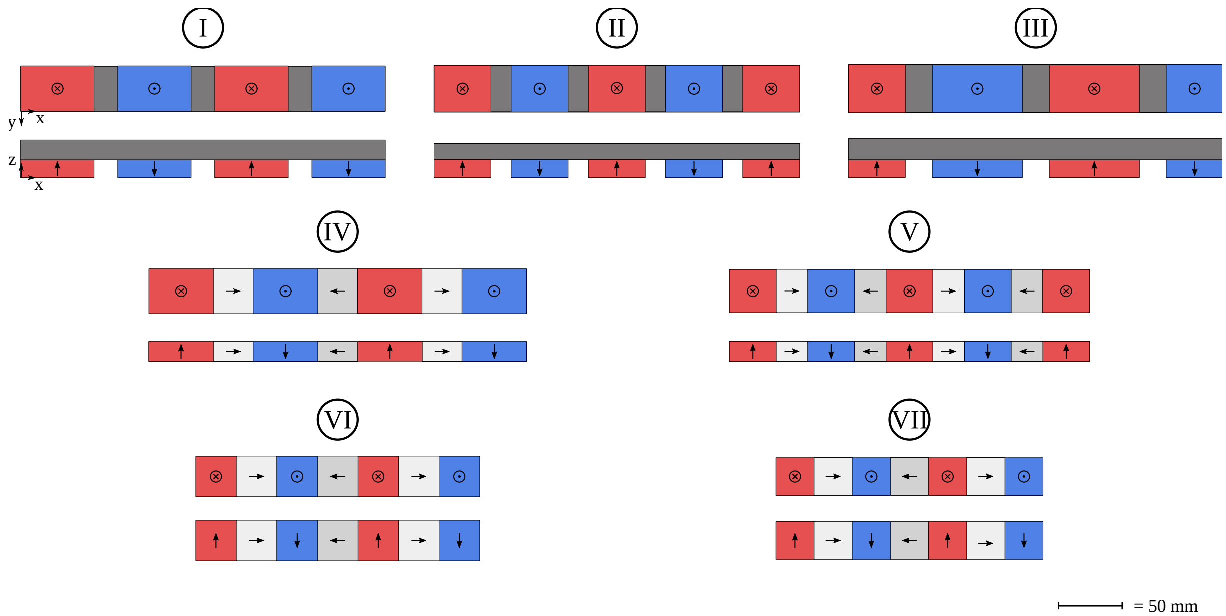

FIGURE 5: *Arrangements resulting from the optimization*

Arrangement	Mass [kg]	LDR – analytical [-]	LDR – FEM [-]
I	2.24	3.14	3.13
II	1.97	2.98	2.96
III	0.86	3.13	3.13
IV	1.25	3.28	3.1
V	1.18	3.1	2.9
VI	1.77	3	2.84
VII	1.42	2.97	2.83

TABLE 3: *LDR and mass of the arrangements selected in the Pareto fronts and comparison between the analytical model and FEM.*

It can be noticed that the Pareto fronts in Figure 4 are quite narrow due to dimensional constraints imposed on the optimization variables but also the dimensions of the track. To alleviate this, an optimization was conducted with no dimensional constraint on the arrangements and with a semi-infinite plate in the xy-plane. The objectives and the lift constraint are kept the same. In Figure 6, the HA is comprised between the AltPM and the AltPM where only the PMs are counted in the mass. The LDRs are higher because of the dimensions and since there is no side track. The fronts are wider and show that the AltPM topology can reach the same performance as the HA when there is less constraints in the optimization.

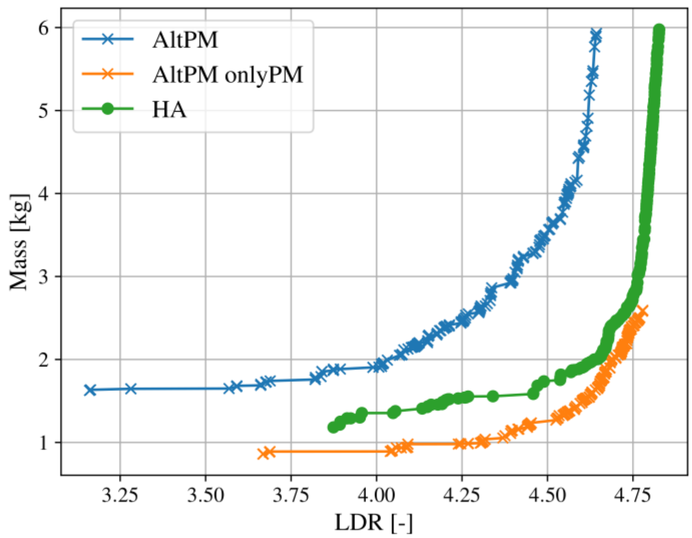

FIGURE 6: *Optimization results with less dimensional constraints and no side track.*

3.2 Parametric analyses

Topologies I, IV and VII have been selected to further compare them using FEM. The lateral gap has been swept between 5 and 30 mm in Figure 7. The optimized HA and AltPM topologies have almost identical performance, even in terms of lateral stiffness. The only difference lies in the ability of the HA to produce slightly larger forces when the lateral gap is small but at the expense of a lower LDR because the magnetic flux density on the side of the HA is larger. However, the HA made of PM cubes generates significantly larger forces and stiffness but a low LDR. As the lateral gap decreases, the PMs come closer the side track which increases only slightly the lift force but more significantly the drag and the guidance force. This results in a lower LDR but greater lateral stiffness. A tradeoff must therefore be found between the two by selecting an appropriate lateral position of the PMs.

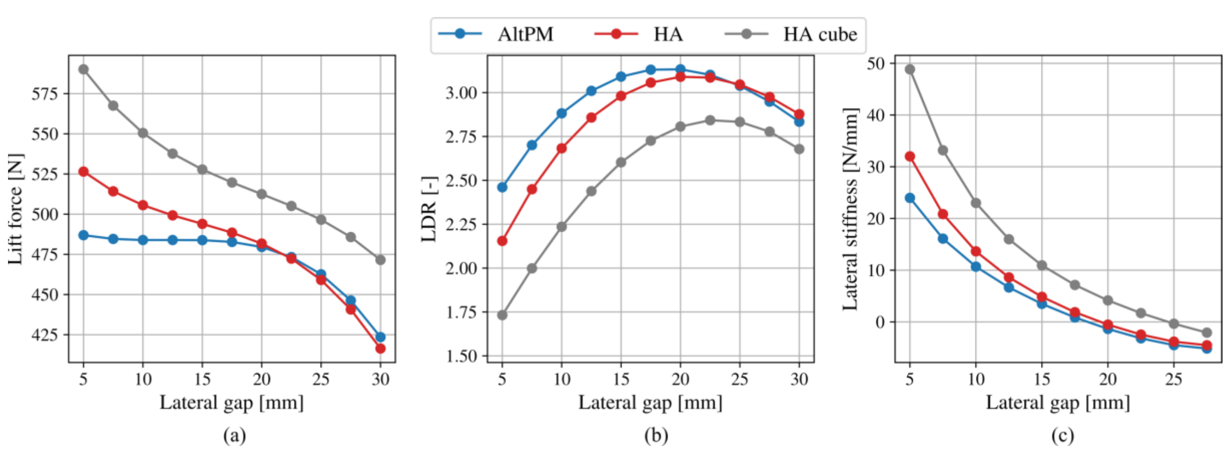

FIGURE 7: *Evolution of (a) the lift force, (b) the LDR, (c) the lateral stiffness with the lateral gap in FEM.*

Figure 8 shows the evolution of the three components of force of the three arrangements with the speed. Since they evolve in the same way, the conclusions drawn in this study should hold for other operating speeds.

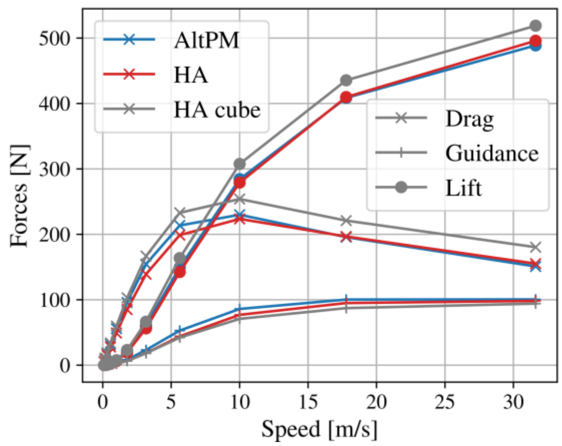

FIGURE 8: *Evolution of the lift, the drag and the guidance force with the speed of the suspension in FEM.*

Finally, the back-iron thickness of the AltPM topology is varied to assess its impact on the forces. The simulations conducted in FEM are non-linear and use stainless steel 430 for the ferromagnetic back-iron. Figure 9 shows the evolution of the forces and the objective functions with the iron thickness. The red zones indicates where the lift constraint is no more satisfied. Indeed, below a certain thickness, the forces drop due to the magnetic saturation between the magnetic poles whereas the LDR is not affected by it. The thickness can be reduced from 16 mm to 12 mm with almost no impact on the performance, which reduces the overall mass of the suspension by 14%.

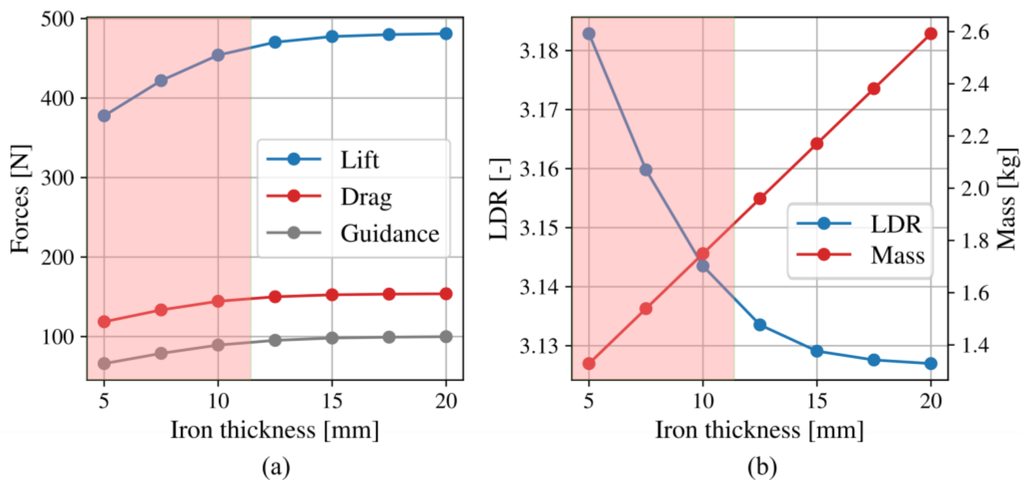

FIGURE 9: *Evolution of (a) the forces, (b) the LDR and the mass with the back-iron thickness using non-linear FEM. In the red zone, the lift constraint (3) is not met.*

The magnetic flux lines close between poles so that the magnetic flux density above the center of a PM is almost equal to zero. The back-iron can therefore be carved in these zones to gain even more weight. Building the back-iron with a superposition of thinner plates, as in Figure 10, can lead to an additional 10% gain on the total mass without degrading the forces. This result was also shown in [9].

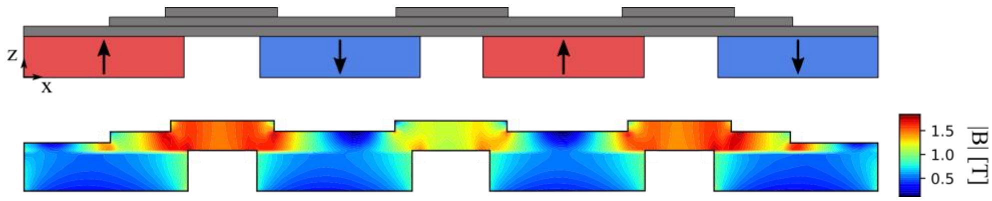

FIGURE 10: *Alternate PM topology with a carved back-iron and the magnetic flux density norm inside it computed with a non-linear FEM simulation considering the eddy current reaction field.*

4. CONCLUSION

This paper optimized and compared the Halbach array and the alternate permanent magnet arrangements of an electrodynamic suspension. The forces generated by both configurations are first modeled analytically in 3-D. The model showed a better accuracy for the alternate topology than the Halbach array but with an error below 7 % in any case. Its limitations could therefore have a slight impact on the results which could be interesting to investigate in further studies. A bi-objective optimization was conducted on the lift-to-drag ratio, the mass of the suspension while respecting constraints linked to application. It is shown that the Halbach array leads to the lowest total mass but both have the same lift-to-drag ratio. However, the alternate permanent magnet configuration can have a lower mass of permanent magnets and therefore potentially a lower cost. Three topologies resulting from the optimization have been further compared by sweeping the lateral position of the permanent magnets and the speed using finite elements, yielding the same conclusions. Finally, a parametric study has been conducted on the thickness of the back-iron of the alternate arrangement to reduce its total weight and come closer to the Halbach array.

ACKNOWLEDGEMENTS

L. Beauloye is a Research Fellow of the Fonds de la Recherche Scientifique (FNRS).

The HES-SO Valais/Wallis also would like to thank the HES-SO for their funding of the GRIPIT project as well as Constellium Valais, YXmagnetic and the city of Sion for their support.

DISCLOSURE OF INTERESTS

The authors have no competing interests to declare that are relevant to the content of this article.

REFERENCES

[1] L. Beauloye and B. Dehez, “Permanent Magnet Electrodynamic Suspensions Applied to MAGLEV Transportation Systems: A Review,” *IEEE Trans. Transp. Electrific.*, vol. 9, no. 1, pp. 748–758, Mar. 2023, doi: 10.1109/TTE.2022.3193296.
[2] Z. Deng *et al.*, “Permanent Magnet Electrodynamic Suspension System Integrated with a Car: Design, Implementation, and Test,” *IEEE Trans. Transp. Electrific.*, pp. 1–1, 2023, doi: 10.1109/TTE.2023.3278946.
[3] M. Flankl, T. Wellerdieck, A. Tüysüz, and J. W. Kolar, “Scaling laws for electrodynamic suspension in high-speedtransportation,” *IET Electric Power Applications*, vol. 12, no. 3, pp. 357–364, 2018, doi: 10.1049/iet-epa.2017.0480.
[4] L. Beauloye and B. Dehez, “Impact of the Magnet Span on the Forces of Electrodynamic Suspensions with an Alternate Permanent Magnet Arrangement,” in *2022 25th International Conference on Electrical Machines and Systems (ICEMS)*, Chiang Mai, Thailand: IEEE, Nov. 2022, pp. 1–5. doi: 10.1109/ICEMS56177.2022.9983125.
[5] M. Fumeaux, M. Cailleteau, D. Melly, S. Chevailler, and J. Cugnoni, “Design and Simulation of the Electrodynamic Suspension of an Hyperloop Test Vehicle,” in *2023 14th International Symposium on Linear Drivers for Industry Applications (LDIA)*, Hannover, Germany: IEEE, Jun. 2023, pp. 1–5. doi: 10.1109/LDIA59564.2023.10297536.
[6] S. Paul and J. Z. Bird, “A 3-D analytic eddy current model for a finite width conductive plate,” *COMPEL: The International Journal for Computation and Mathematics in Electrical and Electronic Engineering*, vol. 33, no. 1/2, pp. 688–706, Dec. 2013, doi: 10.1108/COMPEL-03-2013-0083.
[7] J. W. Jansen, J. P. C. Smeets, T. T. Overboom, J. M. M. Rovers, and E. A. Lomonova, “Overview of Analytical Models for the Design of Linear and Planar Motors,” *IEEE Trans. Magn.*, vol. 50, no. 11, pp. 1–7, Nov. 2014, doi: 10.1109/TMAG.2014.2328556.
[8] M. F. J. Kremers, J. J. H. Paulides, E. Ilhan, J. L. G. Janssen, and E. A. Lomonova, “Relative Permeability in a 3D Analytical Surface Charge Model of Permanent Magnets,” *IEEE Trans. Magn.*, vol. 49, no. 5, pp. 2299–2302, May 2013, doi: 10.1109/TMAG.2013.2239976.
[9] MIT Hyperloop Team, “MIT Hyperloop Final Report,” MIT, 2017.

